European Journal of Pharmaceutical Sciences 211 (2025) 107144

Contents lists available at ScienceDirect

European Journal of Pharmaceutical Sciences

journal homepage: www.elsevier.com/locate/ejps

Hydrogenated plant-based lecithins as excipients for cosmetic and pharmaceutical applications: A physical-chemical study

Fabio Strati [a,†], Simon Drescher [b], Chen Shen [c], Reinhard H.H. Neubert [a], Gerald Brezesinski [a,*]

[a] Institute of Applied Dermatopharmacy at Martin Luther University Halle-Wittenberg, Weinbergweg 23, D-06120 Halle (Saale), Germany
[b] Phospholipid Research Center, Im Neuenheimer Feld 515, 69120 Heidelberg, Germany
[c] Deutsches Elektronen-Synchrotron DESY, Notkestraße 85, 22607 Hamburg, Germany

ARTICLE INFO

Keywords:
Lecithin
Phospholipids
Langmuir monolayers
X-ray scattering
DSC
HLD
Solubility

ABSTRACT

Lecithin is a generic term that is often used to indicate a product mainly constituted of phospholipids. Lecithins can be used in pharmaceutical and cosmetic field as wetting agents, emulsifiers and building blocks for the production of liposomes and micelles. One of its main sources are plants. From their extraction a final product mainly constituted of phosphatidylcholines and phosphatidylethanolamines can be obtained. Common issue connected to freshly extracted lecithins is the presence of a product rich in double bonds subject to photo and air oxidation. By adding in the purification process a further catalytic step, it is possible to form stable hydrogenated lecithin products. Despite their widespread use, little is known about the physicochemical properties of such hydrogenated lecithins, detailed studies mainly based on X-ray scattering methods on mono- and multi-layers have been performed. Additionally, the emulsifying properties of these lecithins such as Hydrophilic-Lipophilic Deviation (HLD parameter) and solubility have also been studied. General findings are that mixtures with higher amounts of phosphatidylcholines (90–100 %) formed a well-defined lamellar phase showing in monolayers complete absence of charge, while lecithins with lower phosphatidylcholine contents (75–80 %) formed charged monolayers and positionally uncorrelated bilayers due to the presence of charged species. The hydrogenated phospholipids (PLs) studied were highly soluble in several co-solvents which are suitable for the incorporation of these phospholipids into relevant dermal formulations. The studied PLs are able to stabilize innovative dermal colloidal formulations such as cerosomes and to improve the incorporation of them into Stratum corneum models.

In conclusion, the following studies will allow a more rational selection of hydrogenated lecithins for the formulation of cosmetic and pharmaceutical products.

1. Introduction

The term lecithin is often used for indicating mixtures of phospholipids (PLs), although lecithin is also indicating mixtures consisting of phospholipids, triglycerides, sterols, fatty acids and glycolipids (Machado et al., 2014; Wendel, 2014). They have been extracted for the first time from egg yolk in 1847 and subsequently from brain, blood, bile, and other organic materials consisting of cell membranes (Gobley, 1850). Since PLs are the structural components of cell membranes, lecithins can be extracted from animal, vegetal and marine sources (Pepeu et al., 1990). Due to their natural surfactant-like properties they can be used as wetting agents, emulsifiers and building blocks for the production of liposomes, lipid nanoparticles, and micelles (Fricker et al., 2010; Van Hoogevest et al., 2011; Fujii et al., 2001; Shinoda and Kaneko, 1988), in particular they find extensive application as excipients for the formulation of macro- and micro-emulsions in dietary, pharmaceutical as well as in cosmetic field (Nastruzzi et al., 1993; Nguyen et al., 2010). One of the main sources of natural PLs are vegetal

Abbreviations: PLs, Phospholipids; PC, Phosphatidylcholine; DPPC, Dipalmitoylphosphatidylcholine; DSPC, Distearoylphosphatidylcholine; PE, Phosphatidylethanolamines; GIXD, Grazing Incidence X-ray Diffraction; GIXOS, Grazing Incidence X-ray Off-specular Scattering; HC, Hydrocarbon Chain; HG, Head Group; TRXF, Total Reflection X-ray Fluorescence; SAXS, Small-Angle X-ray Scattering; DSC, Differential Scanning Calorimetry; SP, Surface Pressure; fwhm, full-width at half-maximum; HLD, Hydrophilic Lipophilic Deviation; CC, Characteristic Curvature.

* Corresponding author.
E-mail address: gerald.brezesinski@iadp.eu (G. Brezesinski).
† present address: Deutsches Elektronen-Synchrotron DESY, CSSB, Notkestraße 85, 22,607 Hamburg, Germany

https://doi.org/10.1016/j.ejps.2025.107144
Received 27 March 2025; Received in revised form 21 May 2025; Accepted 25 May 2025
Available online 26 May 2025

sources such as soybean and sunflower (Perkins, 1995). Final lecithin composition varies according to the method of extraction and purification. The final product is a lecithin fraction that can contain 20–80 % of phosphatidylcholines (PCs) up to 98 % (Van Hoogevest and Wendel, 2014). The fatty acid composition of the PCs is typically palmitic acid (C16:0), stearic acid (C18:0), oleic acid (C18:1), linoleic acid (C18:2), and linolenic acid (C18:3) (Wendel, 2014; Van Hoogevest and Wendel, 2014).

Raw lecithins are unrefined mixtures composed a complex blend of fatty substances, primarily phospholipids, along with triglycerides, glycolipids, free fatty acids, sterols, saccharides, carotenoids, and minor components. PLs extracted from plant based raw lecithins can present technological problems connected with their physicochemical stability. Unsaturated chains have the disadvantage that double bonds are susceptible to air oxidation. Natural lecithin oxidizes readily once exposed to the air forming hydroperoxides and epoxides (FASEB, 2017). Moreover, unsaturated PLs have a phase transition below 0 °C and form at ambient temperature a liquid-crystalline phase (often the L_α phase). Upon hydration, flexible mesophases as hexagonal or cubic structures can be formed (Cevc, 1993). For certain types of PL-based formulations, higher phase transition temperature are preferred for stability reasons (Senior and Gregoriadis, 1982). One easy way to overcome issues connected to stability and low phase transition temperature is hydrogenating the double bonds via catalytic hydrogenation for the formation of fully hydrogenated PLs (Lantz, 1989; Pryde, 1985). Although such hydrogenated PLs mixtures are well described in terms of head group and fatty acid composition, their physicochemical properties are not yet examined in detail to enable a rational selection of the chemically stable lecithin for designing pharmaceutical and cosmetic formulations.

To address the problem of physicochemical characterization, in the following work batches of hydrogenated soybean or sunflower lecithin with different nominal amounts of PCs (70 and ≥ 90 %) were characterised with the application of X-ray scattering techniques studying in parallel monolayer and multilayer systems. Langmuir monolayers are valuable models for evaluation of PLs and membrane biophysics by analysing the two-dimensional ordering of these lipids. A manifold of techniques can be coupled to Langmuir monolayers allowing to observe in detail their behaviour and organization (Dahmen-Levison et al., 2000; Bringezu et al., 2002). In this work, we used highly brilliant light sources for the simultaneous application of Grazing incidence X-ray diffraction (GIXD), Grazing incidence X-ray off-specular scattering (GIXOS) and total reflection X-ray fluorescence (TRXF) (Stefaniu and Brezesinski, 2014) to characterize the hydrogenated lecithins at the air-water interface. The application of Small-Angle X-ray scattering (SAXS) simultaneously to calorimetric analysis will define their organization in bulk dispersions and the thermotropic behaviour of the hydrated lecithin. Finally, solubility properties and the hydrophilic-lipophilic deviation (HLD) parameters of the hydrogenated soybean lecithins have also been estimated. For the determination of the HLD the "Salinity Scan Method", published by Bhakta et al. (Acosta et al., 2008) was used with minor changes. The solubility of the hydrogenated lecithins has been determined for the first time and plays a substantial role for the formation of emulsions and partitioning in pharmaceutically and cosmetically relevant co-solvents of physically stable emulsions. The results of this work will contribute to the characterization of plant-based lecithins which could be used as key components for the stabilization of innovative dermal colloidal formulations such as cerosomes and to improve their incorporation into stratum corneum models.

2. Experimental section

2.1. Materials

The different, purified and hydrogenated PLs (P100–3, S75–3, H100–3, 90 H, and 80 H) used in this study were gently provided by Lipoid GmbH (Ludwigshafen, Germany) and are further detailed in Table 1.

Table 1
Details of PLs used in this study, GMO – Genetically Modified Organisms, the "3″ and the "H" after the number denote hydrogenated PLs.

Label (Lipoid GmbH)	Abbreviation used in this study	Origin	PC content [%]
LIPOID P 100–3	P100–3	non-GMO soybean	≥ 90.0
LIPOID S 75–3	S75–3	soybean	70.0
LIPOID H 100–3	H100–3	non-GMO sunflower	≥ 90.0
PHOSPHOLIPON® 90 H	90 H	soybean	≥ 90.0
PHOSPHOLIPON® 80 H	80 H	soybean	70.0

The typical fatty acid composition can be found in the corresponding data sheets. All hydrated samples were used without further purification.

HPLC grade chloroform and methanol were purchased from VWR International GmbH (Darmstadt, Germany). Millipore water was obtained from Synergy device (Merck, Darmstadt, Germany). $BrCl_2$ was purchased from VWR International GmbH (Darmstadt, Germany).

2.2. Methods

2.2.1. Langmuir monolayer

π–A (Surface Pressure – Area) isotherms were recorded on a computer-interfaced Langmuir-trough (Riegler & Kirstein, Potsdam, Germany) equipped with a Wilhelmy balance using a compression rate of ≤5 cm^2/min (Andreeva et al., 2008). The lecithin mixtures have been dissolved in a solution of chloroform with a final concentration of 1 mg/ml. The solutions were stored at 4 °C for a maximum of 2 weeks in dark environment. Millipore water was used for subphase preparation. Each isotherm was recorded at room temperature (≃ 20 °C).

2.2.2. GIXD

GIXD experiments were performed at the beamline P08 (PETRA III of Deutsches Elektronen-Synchrotron DESY, Hamburg, Germany) at an incident energy of 15 keV (wavelength λ = 0.827 Å) and an incident angle of 0.07° with respect to the water surface (Seeck et al., 2012). The details of the measurements have been described elsewhere (Pusterla et al., 2022) and only the key parameters are given here. The beam size was 70 μm (vertical) × 1000 μm (horizontal), providing an X-ray footprint of 50 × 1 mm^2 at the chosen incidence. The Langmuir trough (Riegler & Kirstein, Potsdam, Germany) was placed in a hermetically sealed container, which was constantly flushed with pre-humidified Helium (He). The temperature of the trough was kept at (20 ± 0.1) °C. The diffraction signal was collected by a vertically-oriented position-sensitive detector (MYTHEN2 1 K, DECTRIS, Baden, Switzerland) after a Soller collimator (JJ X-RAY, Denmark), providing an in-plane angular resolution of 0.08° (full-width at half-maximum, fwhm). The diffraction data consist of Bragg peaks in the 2-dimensional intensity vs. (Q_{xy}, Q_z) space. The visualization of the diffraction peaks was performed using an in-house written python macro. To obtain the information on the monolayer structure, i.e. chain lattice parameters, tilt angle t, distortion d, cross-sectional area (A_0) and the in-plane lattice area of one chain (A_{xy}), the collected diffraction peaks were analyzed using a procedure established earlier (Kjaer et al., 1987; Kjaer, 1994). The diffracted intensity was integrated over a defined vertical Q_z window and over a horizontal Q_{xy} window to obtain Bragg peaks (I vs. Q_{xy}) and Bragg rods (I vs. Q_z), respectively. These curves were further modelled with 1-dimensional Gaussian functions in Q_z-direction and 1-dimensional Lorentzian functions in Q_{xy}-direction, accordingly. The obtained Bragg peak and rod positions and their corresponding fwhm allowed to extract information on the monolayer structure. In order to take the in-plane

divergence of the X-ray beam into account, the fwhm of the Lorentzian peaks were corrected as follows:

$$fwhm_{xy}^{cor} = \sqrt{\left(fwhm_{xy}^{meas}\right)^2 - \left(fwhm_{xy}^{res}\right)^2},\ with\ fwhm_{xy}^{res} = 0.0122\ \mathring{A}^{-1}.$$

The correlation length of the formed domains was then deduced as: $L_{xy} = \frac{2}{fwhm_{xy}^{cor}}$ for Lorentzian shape diffraction peak (Kaganer et al., 1999).

2.2.3. GIXOS

GIXOS yields the electron density profile of the lipid layer in the direction perpendicular to the liquid/air interface. The details of this technique are described elsewhere (Wiegart et al., 2005; Dai et al., 15 November 2011). Briefly summarized, the Q_z-dependence of the diffuse scattering intensity $I(Q_{xy}, Q_z)$ recorded at a low-enough but non-zero value of Q_{xy} contains information equivalent to that of the conventional reflectivity $R(Q_z)/R_F(Q_z)$. In the present work, the GIXOS signal was measured at an angle of 0.30° off from the plane of incidence, selected by horizontally offset two post-sample slits (Dai et al., 15 November 2011), and this corresponds to $Q_{xy} = 0.04$ Å^{-1} at horizon.

The experimental data were analyzed with slab models of the interfacial electron density profiles (see Results section and Supporting Information). These profiles were treated with the Parratt formalism to obtain the theoretical reflectivity, $R(Q_z)$, which was then transformed by multiplication with $V(Q_z)/R_F(Q_z)$ to obtain the theoretical GIXOS signal. $V(Q_z)$ is the Vineyard function and $R_F(Q_z)$ is the Fresnel reflectivity of an ideal interface between the two bulk media. The best-matching layer parameters were obtained by χ^2-minimization of the deviation between the experimental and theoretical GIXOS data. Here, the Q_{xy} dependence of the capillary wave model in the modeling is neglected since it will only result in an apparently sharper interface, but not affect the thickness and density evaluation within the experimental accuracy (Pusterla et al., 2022; Shen et al., 2024).

2.2.4. TRXF

In recent years, TRXF has been established as an element-specific complementary scattering technique (Shapovalov et al., 2007; Brezesinski and Schneck, 2019). The TRXF measurements were carried out at beamline P08 (PETRA III, DESY, Hamburg, Germany) using the above described set-up. The fluorescence signal was detected by an Amptek XR-100SDD detector (Amptek, Bedford, USA) placed almost parallel to the liquid surface and perpendicular to the photon beam axis. This detector position was chosen in order to keep the Compton scattering at the given polarization of the photons as low as possible. The footprint centre of the incident beam was adjusted to the middle of the trough at the middle of the view angle of the fluorescence detector (Brezesinski and Schneck, 2019; Sturm et al., 2019).

2.2.5. SAXS

X-ray scattering experiments were performed in transmission geometry using a Retro-F laboratory setup (SAXSLAB, Massachusetts) equipped with a microfocus X-ray source (AXO Dresden GmbH, Germany) with an ASTIX multilayer X-ray optics (AXO Dresden GmbH, Germany) as monochromator for Cu-K_α radiation ($\lambda = 1.54$ Å). Measurements were recorded in vacuum using a PILATUS3 R 300 K detector (DECTRIS Ltd., Switzerland). As sample holder borosilicate glass capillaries (WJM-Glas, Berlin, Germany) with a diameter of 1 mm were used. The samples were prepared as 1:4 w/w lipid/water systems. To equilibrate the sample, consecutive cycles of heating and vortexing were completed. The measurements were performed at room temperature and the scattered signal was collected at two/three sample-to-detector distances to cover a larger effective Q-range from 0.01 Å^{-1} to about 3 Å^{-1}. As a reference sample for calibration purposes silver behenate was used. All scattering patterns were background corrected and azimuthally averaged to give one-dimensional scattering intensity curves. Each diffraction pattern is presented as normalized scattering intensity in arbitrary units versus the scattering vector Q ($Q = (4\pi \sin\theta)/\lambda$), where θ is half the diffraction angle). Lorentzian functions were fitted to the diffraction peaks obtained. From the peak maximum positions of the small-angle diffraction patterns, the repeat distances D ($D = 2\pi/Q$) were defined.

2.2.6. Differential scanning calorimetry

The differential scanning calorimetry (DSC) measurements were performed on a MicroCal VP-DSC calorimeter (MicroCal Inc., Northampton, MA). Each PL sample was dispersed in water at a concentration of 2 mg/ml. The scanned temperature range was between 15 and 75 °C, the heating rate was 60 °C/h, and each heating and cooling scan was repeated to confirm reproducibility. The first scan was discarded. The reference cell was filled with pure water. DSC scans were evaluated using MicroCal Origin 8.0 software.

2.2.7. Solubility studies

The solubility of the samples in the co-solvents and oils has been estimated because it is substantial for the formation of physically stable emulsions. The solubility was measured by stepwise addition of the corresponding solvent to a given mass of compound. Samples were then heated to 75 °C for 15 min and stored for 48 h at room temperature before visual examination.

2.2.8. HLD determination

The two most well-known alternatives to the hydrophilic–lipophilic balance (HLB) parameter are the critical packing parameter (CPP) (Otto et al., 2020) and the hydrophilic-lipophilic deviation (HLD) (Tadros, 2016; Abbott, 2015/2016). The HLD-concept is far more complex than the CPP as it includes the electrolyte concentration (Salinity S) of the aqueous phase as well as the type of oil used in the emulsion (Equivalent Oil Alkane Carbon Number EACN), and a correction term for the temperature dependence (α): HLD = F(S) - k·EACN - α·(T – 25) + CC. CC is called characteristic value for the hydrophobic/hydrophilic nature of the surfactant. The salinity function F(S) is relevant for ionic surfactants, whereas the temperature (T) is more relevant for non-ionic ethoxylated surfactants.

3. Results and discussion

3.1. Monolayer studies

Lecithins as natural products find extensive application in pharmaceutical and cosmetic fields. The composition of commercially available lecithins from plant sources consists of a lipid fraction enriched in particular with unsaturated PCs. Since these products feature stability issues, an extra hydrogenation step can be performed to produce samples with exclusively saturated hydrocarbon chains that have higher melting temperatures and are stable against oxidation (Van Hoogevest and Wendel, 2014). Since the physicochemical properties of these hydrogenated plant-based lecithins were not yet described, the main objective of this work was to characterize several hydrogenated samples with different amounts of PC and compare their properties with those of the corresponding non-hydrogenated PL mixtures. One widely used method for such studies are Langmuir monolayers which are useful tools for the study of biological membranes since a bilayer can be considered as two weekly coupled monolayers (Brezesinski and Möhwald, 2003; Stefaniu et al., 2014; Möhwald and Brezesinski, 2016).

First, the Langmuir monolayer experiments were carried out in order to characterize the phase behavior of the corresponding monolayers at constant temperature. The π-A compression isotherms are presented in Fig. 1. The surface pressure (π) was plotted against the total area (A) of the trough (Fig. 1a) since the composition of the samples is not well-defined and therefore, a precise molecular weight cannot be calculated. Samples with higher amount of PC (H100–3, 90 H and P100–3) showed stiffer isotherms (a larger slope dπ/dA is characteristic for monolayers with a large lateral compression modulus K) in comparison

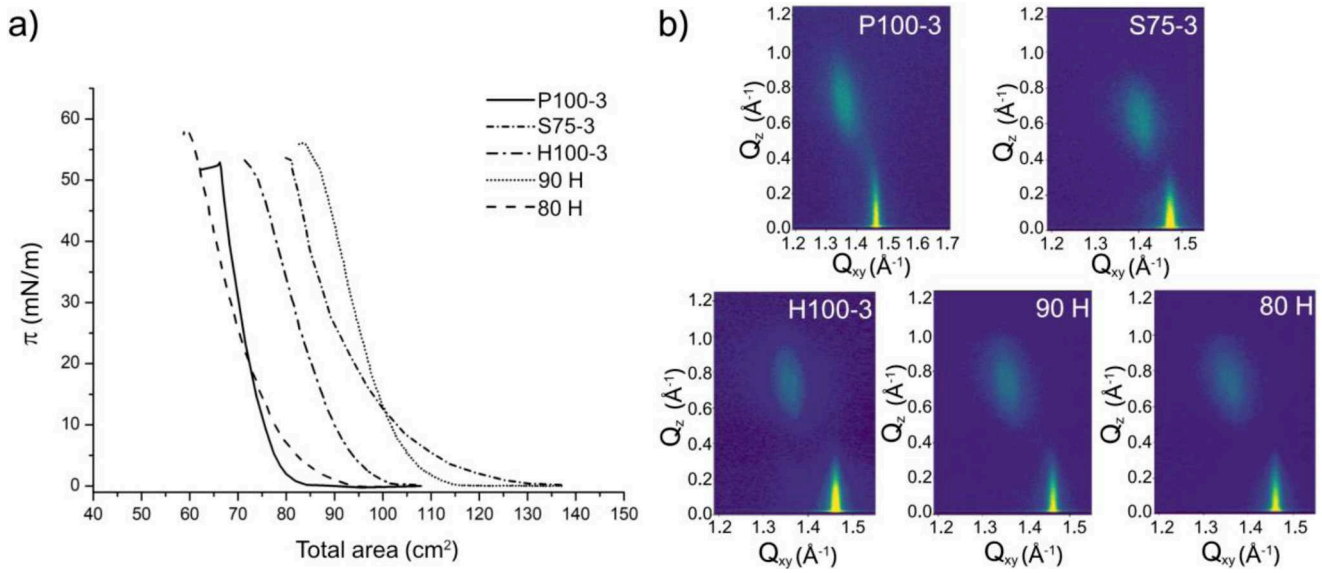

Fig. 1. a) π-A (here total area) isotherms of hydrogenated lecithins on Millipore water at 20 °C and b) GIXD contour plots of lecithin mixtures recorded at 30 mN/m at 20 °C on 5 mM $CaBr_2$. The clearly visible two diffraction peaks describe a rectangular unit cell of NN (nearest neighbor) tilted chains.

to 80 H and S75–3 containing a lower percentage of PC. However, even these monolayers were stiffer than the corresponding non-hydrogenated samples (Otto et al., 2018). The isotherms of all five hydrogenated samples are typical for fully-condensed monolayers. No phase transitions, indicated by a plateau (first-order phase transition between liquid and solid monolayers) or kink (second-order phase transition between two condensed phases), can be seen in the isotherms demonstrating that at practically zero pressure condensed and gas-analogous phases do co-exist. Above the lift-off pressure (re-sublimation) only a condensed phase is present. A direct comparison with DPPC (1,2-dipalmitoylphosphatidylcholine) and DSPC (1,2-distearoylphosphatidylcholine), the main components in the used samples, showed that the investigated hydrogenated lecithins are far more similar to DSPC which also does not exhibit a phase transition at 20 °C, whereas DPPC has a first-order transition from a liquid-like state to a condensed one at ~6 mN/m (Hao et al., 2016; Kuzmenko et al., 2001). This is surprising since the used lipids are multi-component systems. Obviously, the lipids with the C18-chains dominate the phase behaviour and the other lipids of these mixtures are incorporated with no evidence of phase separation.

X-ray scattering methods were applied to study the organization of the lipids in condensed monolayers at the liquid/gas interface. GIXD is a powerful technique where the diffracted beam allows to generate a diffraction pattern where the monolayer can be considered as a 2D powder of crystallites confined to the subphase surface (Kjaer et al., 1987; Kjaer, 1994; Kuzmenko et al., 2001). Depending on the lattice type, the GIXD pattern presents different number of Bragg peaks. Each

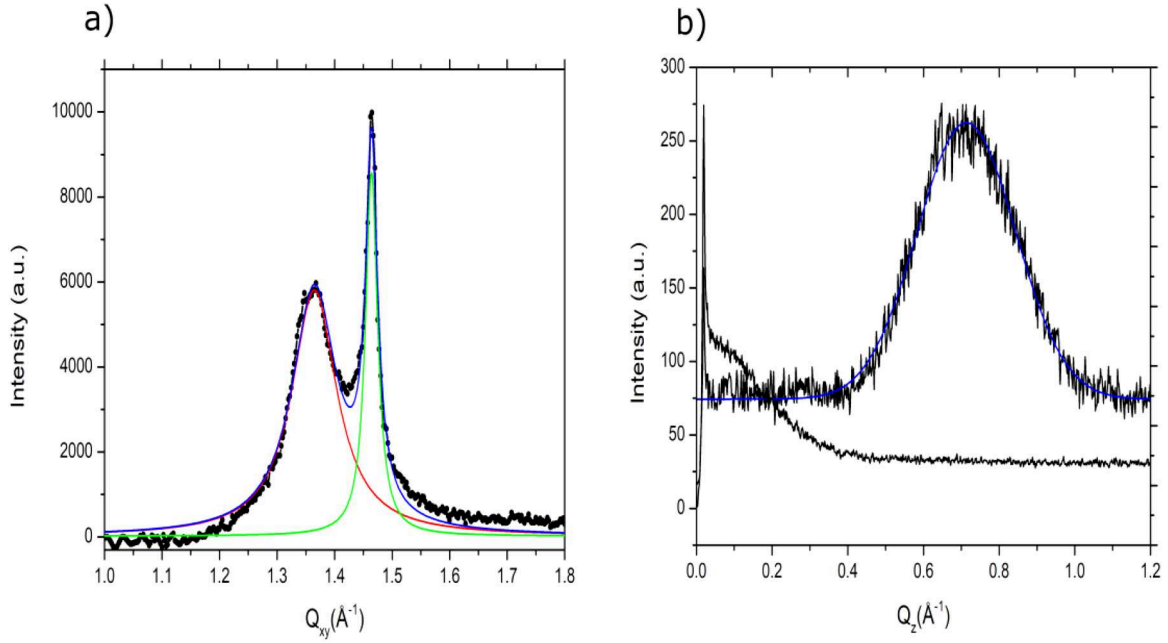

Fig. 2. Scattered intensity of the P100–3 monolayer versus the in-plane scattering component Q_{xy} (a) and versus the out-of-plane scattering component Q_z (b). Note, that the intensity of the degenerated peak in (b) has been scaled by a factor of 5 for clarity. The fitting of Lorentzian functions (Bragg peaks) and Gaussian functions (Bragg rods) to the experimental data is illustrated.

diffraction peak is described by an in-plane component (Bragg peak, Q_{xy}) and an out-of-plane component (Bragg rod, Q_z).

An example of data analysis is presented in Fig.2. The GIXD parameters measured at 30 mN/m are presented in Table 2 (the data measured at different pressures are presented in Table S1, supporting information). For simplification, all studied lipids have been described with the same type of lattice (Fig. 1b), a NN tilted centred rectangular unit cell with one non-degenerate Bragg peak located at the horizon ($Q_z = 0$) and a second degenerate Bragg peak found above the horizon ($Q_z > 0$). The same type of unit cell can be found for DSPC and DPPC. A more detailed analysis indicates the formation of an oblique lattice with two peaks at higher Q_z, which are very close to each other, and the peak close to the horizon has a Q_z values slightly above zero (Estrela-Lopis et al., 2004). The chains are strongly tilted in NN direction. For all sample, the non-degenerate peak is located at 1.46–1.47 Å^{-1} and the degenerate peak between 1.36–1.41 Å^{-1}. These values are similar to those of DSPC and DPPC with 1.46–1.47 Å^{-1} and 1.35–1.39 Å^{-1} at 30 mN/m (Estrela-Lopis et al., 2004; Brezesinski et al., 2001). The calculated cross-sectional area of the hydrocarbon chains was $A_0 \simeq$ 19.8–19.9 Å^2 indicating tight packing of chains in all-*trans* conformation with small rotational liberty. The tilt angle for the mixtures H100–3, 90 H and P100–3 had very similar values at 30 mN/m ($\simeq$ 32–33°), in contrast to the smaller values observed for 80 H and S75–3 (approximately 30° and 27°, respectively).

As usually found for amphiphilic monolayers, the tilt angle of the hydrocarbon chains decreased by increasing the lateral pressure π. By plotting 1/cos(t) against π (Fig. 3a) and extrapolating to 1/cos(t) = 1, the lateral pressure at which the lipid chains become non-tilted can be determined (Bringezu et al., 2002). The pressure needed to reach the non-tilted state was above 73 mN/m for all samples with high PC content (P100–3, H100–3, 90 H). Such a transition pressure is clearly above the values which can be reached by compressing the layer without collapsing it. In contrast, the samples 80 H and P75–3 with much lower PC content reach the transition pressure between 60 and 70 mN/m. Especially 80 H with a transition pressure of ~60 mN/m could be theoretically compressed into the non-tilted state. The tilt angle at zero pressure is with ~40° the same for all samples with high PC content. Smaller values have been observed for 80 H (36°) and S75–3 (35°). The higher non-PC content in the samples allows tight packing with lower tilt angles.

A linear dependence of the lattice distortion d from sin^2t (Fig. 3b) was deduced from a modified Landau theory, which predicts that the tilt contribution to the distortion is proportional to sin^2t with t as the tilt angle of the chains (Kaganer et al., 1999). By extrapolating to sin$^2t = 0$, it was possible to find the d_0-value that is a measure of the contribution of chain backbone ordering to the lattice distortion additionally to the chain tilt. For all samples, the d_0 was found to be slightly negative (mostly −0.03). This small deviation from zero shows that the distortion is mainly caused by the tilt of the molecules with a certain contribution from an ordering of the chain backbones. This is surprising and in contrast to synthetic pure PCs as DPPC and DSPC. Obviously, the packing in the investigated mixtures is slightly different to that in pure PC monolayers.

Last but not least, the two-dimensional compressibility χ, defined as $\chi = -A^{-1}(dA/d\pi)$, can be determined from the slope of the isotherm at constant temperature. The reciprocal quantity is the lateral compression modulus $K_a = 1/\chi = -A(d\pi/dA)$. Additionally, the dependence of the Q_{xy} values of the diffraction peaks on the lateral pressure π gives information about the lateral compression modulus K_c. In the present case, all samples form monolayers with a rectangular unit cell. Therefore, the linear compressibility along each diffraction vector Q_{hk} can be determined as $\chi = (1/Q_{hk})(dQ_{hk}/d\pi)$.

Fig. 4 (left) presents the pressure dependencies of the positions of the two diffraction peaks Q_{02} and Q_{11}. The two peaks respond quite differently to the applied pressure: the position of the non-degenerate Q_{02} peak remains almost unchanged within the accuracy of the measurements, while that of the degenerate Q_{11} peak increases remarkably with increasing pressure. Based on the pressure dependence of the diffraction peak positions, the compression moduli K_c are also quite different in the different directions. In tilt direction (along Q_{11}), K_c is quite low and with values between 300 and 400 mN/m similar to K_a determined from the π/A-isotherms. In contrast, the K_c values perpendicular to the tilt direction (along Q_{02}) are 10-fold or more bigger (2 – 6 N/m). Such values are similar to those observed for the single-chain octadecanol with an extremely small head group in the mesophase phase S (Brezesinski et al., 1998; Kaganer et al., 1998). This phase is characterized by centred rectangular packing of untitled molecules and has one-dimensional periodicity. The compressibility in this phase is also anisotropic. For monolayers undergoing the direct transition from the gaseous phase to a condensed phase (re-sublimation), the condensed islands are already formed during spreading. Both K_c do practically not change with compression, indicating that the packing density of such condensed layers is almost not influenced by compression. This can be easily understood since the monolayers respond to the compression either by changing the tilt angle (low and almost constant K_c) or by keeping the high packing density perpendicular to the tilt direction (high and almost constant K_c). Additionally, K_a is also influenced by the defects produced during the spreading procedure. Since only isotropic compression can be applied to a monolayer powder sample, K_a cannot be larger than the smallest K_c (Le Chatelier principle) in a sample with rectangular unit cells.

In parallel to GIXD, GIXOS was applied in order to obtain information about the laterally averaged electron density perpendicular to the surface giving information about the dimensions of the hydrophobic and hydrophilic parts of these thin films. The GIXOS signals recorded with the used hydrogenated lipid monolayers at 30 mN/m are presented in Fig. S2. The solid lines indicate the theoretical GIXOS signals according to the best-matching model parameters presented in Table 3. Right next to the GIXOS curves, the reconstructed scattering length density profiles SLD = $\rho_e(z)\cdot r_e$ (with r_e = 2.818 fm as the classical electron radius) corresponding to the data in Table 3 are shown. A two-slab model $\rho_e(z)$ has been used before accounting for interfacial roughness. One slab describes the hydrocarbon chain (HC) layer with a slightly too high electron density ($\rho_{HC} \approx$ 0.34 - 0.35 e$^-$/Å^3) for H100–3, 90 H and 80 H, and the expected moderate values of $\rho_{HC} \approx$ 0.32 e$^-$/Å^3 for P100–3 and S75–3. The slightly too high ρ_{HC} could be connected with the slightly too low interfacial roughness $\sigma_{air/HC}$ (see Table 2). The values for the samples with unsaturated chains (P100 and S75) are even smaller ($\rho_{HC} \approx$ 0.3 e$^-$/Å^3 due to the lower packing density in a HC layer with many *gauche* defects. The layer with higher electron density ($\rho_{HG} \approx$ 0.41 - 0.43 e$^-$/Å^3 for the saturated samples) accommodates the head groups (HG).

The thickness of the HC layer of the hydrogenated phospholipids was found between 15.7–16.6 Å, while the head group layer had a thickness

Table 2
Bragg peak (Q_{xy}) and Bragg rod (Q_z) positions of the studied lipid monolayers as well as the corresponding lattice parameters (a, b, c and α, β, γ), tilt angle (t), lattice distortion (d), cross-sectional area (A_o) and in-plane chain area (A_{xy}) extracted from the GIXD data. The monolayers are prepared on $CaBr_2$ solution at 20 °C and measured at 30 mN/m or 25 mN/m (S75–3).

lipid	$Q_{xy}(1)$ [Å^{-1}]	$Q_z(1)$ [Å^{-1}]	$Q_{xy}(2)$ [Å^{-1}]	$Q_z(2)$ [Å^{-1}]
P100–3	1.36	0.72	1.46	0
S75–3	1.41	0.62	1.47	0
H100–3	1.36	0.74	1.46	0
90 H	1.36	0.76	1.46	0
80 H	1.39	0.69	1.47	0

lipid	a [Å]	$b = c$ [Å]	α [°]	$\beta=\gamma$ [°]	t [°]	d	A_{xy} [Å^2]	A_0 [Å^2]
P100–3	5.48	5.09	104.8	122.6	32.1	0.101	23.5	19.9
S75–3	5.22	5.01	117.2	121.4	27.3	0.056	22.3	19.8
H100–3	5.48	5.10	115.1	122.5	32.8	0.097	23.6	19.8
90 H	5.48	5.10	115.1	122.5	33.5	0.097	23.6	19.6
80 H	5.33	5.04	116.2	121.9	30.3	0.076	22.8	19.7

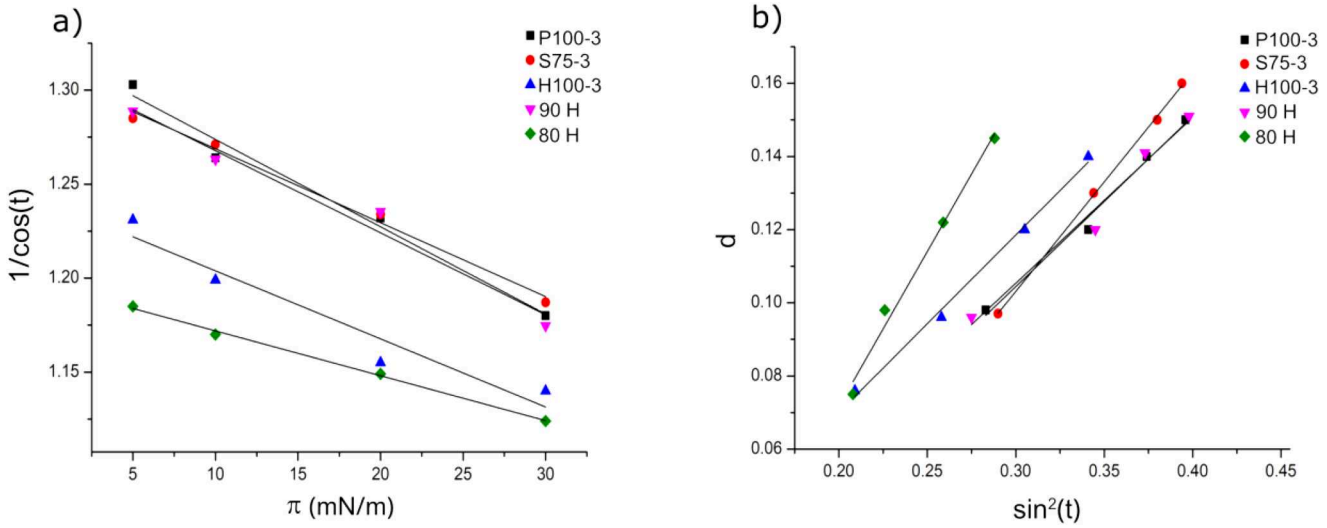

Fig. 3. a) 1/cos(t) vs. surface pressure. t is the tilt angle of the hydrocarbon chains determined by GIXD. The linear extrapolation yields the pressure of the tilting transition and the tilt angle at zero pressure. b) Lattice distortion d vs. $\sin^2(t)$. The linear extrapolation yields the value of d_0 that is a measure of the contribution of chain backbone ordering to the lattice distortion.

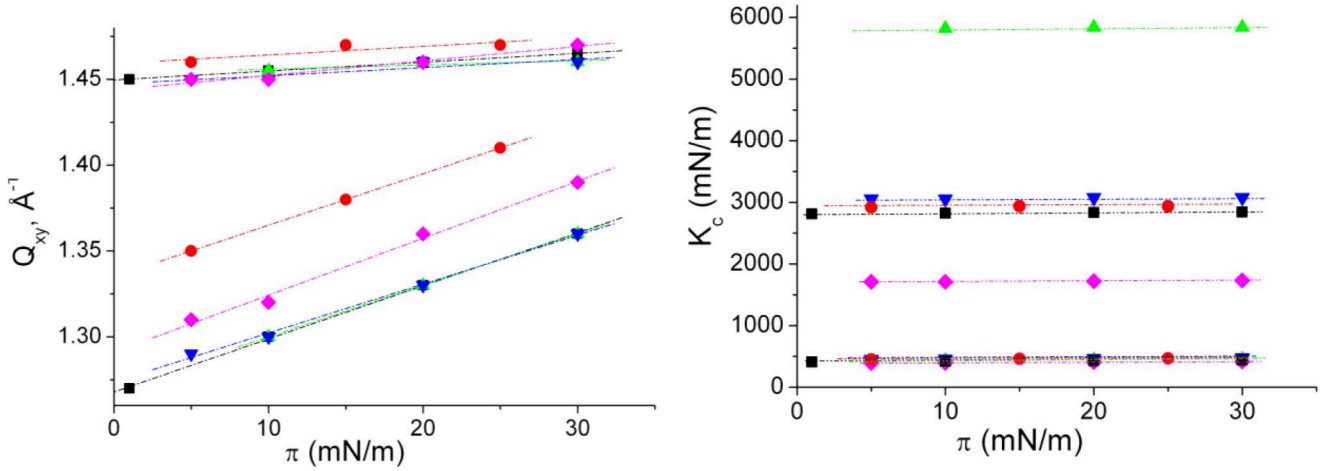

Fig. 4. Left) Pressure dependence of the positions Q_{xy} of the (02) and (11) diffraction peaks of H100–3 (▲), 90 H (▼), 80 H (♦), P100–3 (■) and S75–3 (●). Right) The compression modulus K_c along the diffraction vectors Q_{02} and Q_{11} of H100–3 (▲), 90 H (▼), 80 H (♦), P100–3 (■) and S75–3 (●).

Table 3
Parameters of the HC and HG layers in the electron density profiles of the lipid monolayers as obtained by GIXOS.

lipid	H100–3	90 H	80 H	P100–3	S75–3	P100	S75
d_{HC} [Å]	15.7 ± 0.1	15.7 ± 0.1	16.0 ± 0.1	15.7 ± 0.2	16.6 ± 0.1	12.3 ± 1.6	12.9 ± 0.1
d_{HG} [Å]	9.1 ± 0.1	9.0 ± 0.1	9.4 ± 0.1	9.1 ± 0.4	9.1 ± 0.3	8.7 ± 0.4	8.8 ± 0.4
$\sigma_{air/HC}$ [Å]	2.0 ± 0.1	2.1 ± 0.1	2.2 ± 0.1	2.3 ± 0.1	2.1 ± 0.1	2.4 ± 0.1	2.4 ± 0.1
ρ_{HC} [e^-/Å^3]	0.339 ± 0.004	0.347 ± 0.004	0.358 ± 0.004	0.318 ± 0.004	0.320 ± 0.011	0.300 ± 0.007	0.296 ± 0.011
ρ_{HG} [e^-/Å^3]	0.429 ± 0.004	0.433 ± 0.004	0.436 ± 0.004	0.412 ± 0.007	0.405 ± 0.007	0.394 ± 0.014	0.387 ± 0.011

between 9 and 9.4 Å. GIXOS experiments performed with the unsaturated lecithins show a smaller HC layer thickness (12 - 13 Å) but a rather similar HG layer thickness (∽8.7 Å).

Even if GIXOS is a pseudo-reflectivity method, the results are in good agreement with the GIXD data. Using the Scherrer formula (0.9·2π/fwhm), the full-width at half-maximum (fwhm) of the Bragg rod allows an estimation of the length of the scattering unit (alkyl chain length). For all five hydrogenated samples a value of ∼19 Å was found. This value is close to the theoretical length of a C16 chain (20.4 Å). Taking the measured by GIXD tilt angle (∼32°) of the chains into account, a HC layer thickness of ∼17 Å has been obtained. This value is in good agreement with the value obtained by GIXOS.

Finally, TRXF was used to identify the ions attracted to the monolayer at the air-water interface. This technique allows to quantify the concentration of ions close to the monolayer by detecting their fluorescent signal (Shapovalov et al., 2007; Brezesinski and Schneck, 2019). To study the electrostatic properties of the studied lecithin monolayers, an aqueous subphase containing 5 mM of $CaBr_2$ was used and non-hydrogenated and hydrogenated mixtures were compared. Fig. 5 presents the unsubtracted (the baseline of the subphase was not subtracted) part of TRXF spectra of the phosphate and calcium region of Langmuir monolayers composed of P100–3 and S75–3 (Fig. 5a) as well as of H100–3, 90 H, and 80 H (Fig. 5b) on the $CaBr_2$ subphase. The intensities of the Kα and Kβ lines of the calcium (Ca^{2+}) signal (Kα = 3.69 keV, Kβ = 4.01 keV) and the P signal (Kα = 2.01 keV, Kβ = 2.14 keV) are of great interest. For the samples P100–3, H100–3, and 90 H, the Ca^{2+} signal intensities are of the same intensity as the background indicating the absence of charge in these monolayers. In contrast, the S75–3 and 80 H mixtures, both with a lower PC content, have clearly stronger Ca^{2+} signals compared to the previously discussed ones. The presence of Ca^{2+}ions at the interface shows that these monolayers are negatively charged. Since PCs are zwitterionic lipids at pH 7, the absence of charge in mixtures with ≥ 90 % of PCs was an expected behaviour. The samples with much lower PC content (S75–3 and 80 H) contain obviously anionic species which generate the negative charge attracting Ca^{2+} ions from the subphase. The hydrogenation does not change the negative charge (same intensities of Ca lines) of the corresponding monolayers. However, the P signal is clearly larger in the layers of P100–3 and S75–3 compared to the non-hydrogenated samples P100 and S75 (see SI) showing that the packing density in the hydrogenated samples is much higher. The proven charge of the monolayers of S75–3 and 80 H is in perfect agreement with the described SAXS profiles which will be discussed later.

3.2. Multilayer studies

3.2.1. SAXS

Although monolayers are very useful models for studying PL membranes, the opposing layer of a bilayer, as one of the most important self-assembled structures in nature, is missing. Cell membranes of almost all organisms and many viruses are made of a lipid bilayer. Therefore, the hydrogenated lecithin mixtures were also studied in bulk using SAXS allowing to determine and quantify the bilayer structure in the used mixtures.

The SAXS profiles of the different hydrogenated mixtures varied with the different compositions of PCs. H100–3, 90 H and P100–3 formed a clearly pronounce lamellar phase (Fig. 6 and Table 4) with 4 to 5 orders of reflections, dominated by the high PC content. H100–3 and 90 H have almost the same *d*-spacing of 68.3 - 69 Å each, whereas P100–3 has with 62.2 Å a much smaller *d*-value. Compared with the monolayer results (GIXD and GIXOS), which are quite similar for these mixtures, the significantly thinner bilayer of P100–3 is surprising and must be based on different chain lengths composition and the influence of non-PC compounds. Furthermore, the *d*-spacings of the investigated mixtures can be compared with those of the main components of these mixtures: DPPC and DSPC (63.4 and 67.0 Å, respectively) (Bryant et al., 2019; Lúcio et al., 2008). The direct comparison with the non-hydrogenated P100 soybean lecithin mixtures, with a *d*-spacing of 61.6 Å (Otto et al., 2018), indicates that the hydrogenation, which leads to the formation of stiffer chains (all-*trans* conformation), has almost no influence on the *d*-values. Since the head group composition is the same, a similar thickness of the water layer between the bilayers can be assumed. The formation of all-*trans* conformation with larger distances between the CH_2-groups (Israelachvili, 2015; Mukhina et al., 2022) (larger chain length) is obviously compensated by the tilt of the chains. To conclude, these results suggested that the samples H100–3 and 90 H were able to incorporate more water between the bilayers leading to larger *d*-spacing compared to P100–3.

Contrary to the mixtures composed mainly of PCs, S75–3 and 80 H show scattering profiles with much higher complexity. The absence of defined Bragg peaks and the specific modulation of the scattering intensity suggests the formation of positionally uncorrelated bilayers and might indicate the presence of a small amount of charged species in agreement with the TRXF data described above (Pozo-Navas et al., 2003;

Table 4
The *q*-values of the 1st-order reflection of the lamellar phases of studied mixtures (indicated) with the corresponding *d*-values as obtained by SAXS. Additionally, the fwhm and the number of observed reflections are given.

lipid	*Q* [Å^{-1}]	*d* [Å]	*fwhm* [Å^{-1}]	*orders*
H100–3	0.092	68.3	0.026	5
90 H	0.091	69.0	0.039	5
P100–3	0.101	62.2	0.018	4

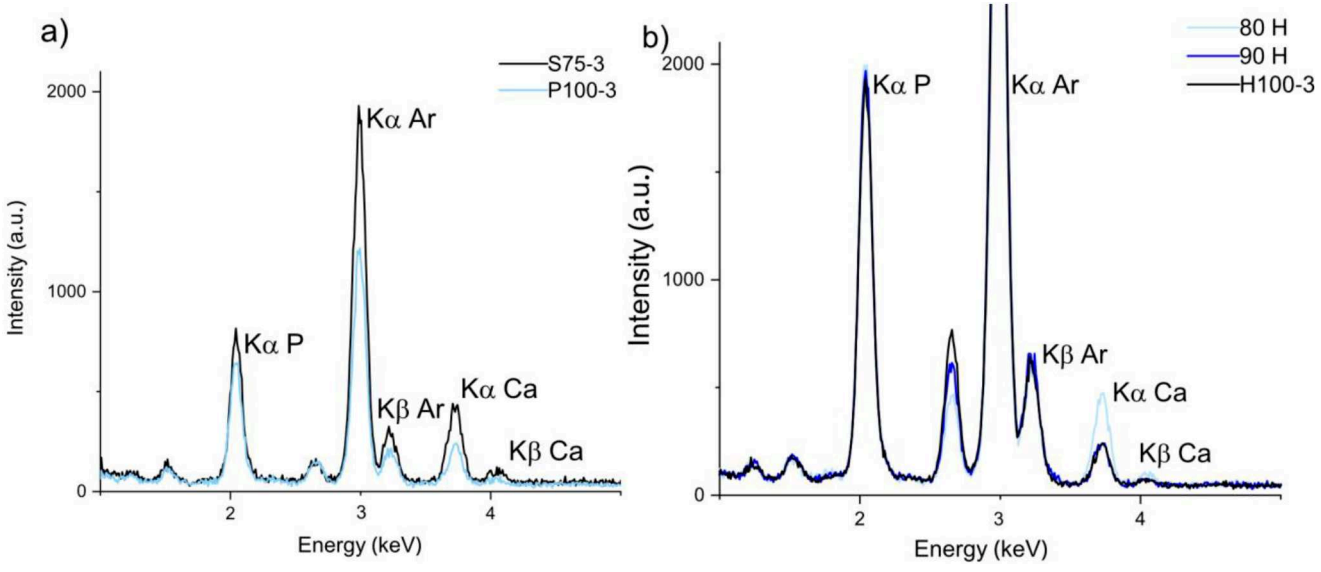

Fig. 5. TRXF spectra (fluorescence intensity vs. photon energy) of monolayers of the investigated mixtures (indicated) on subphases containing 5 mM $CaBr_2$. The region shows the P and Ca lines.

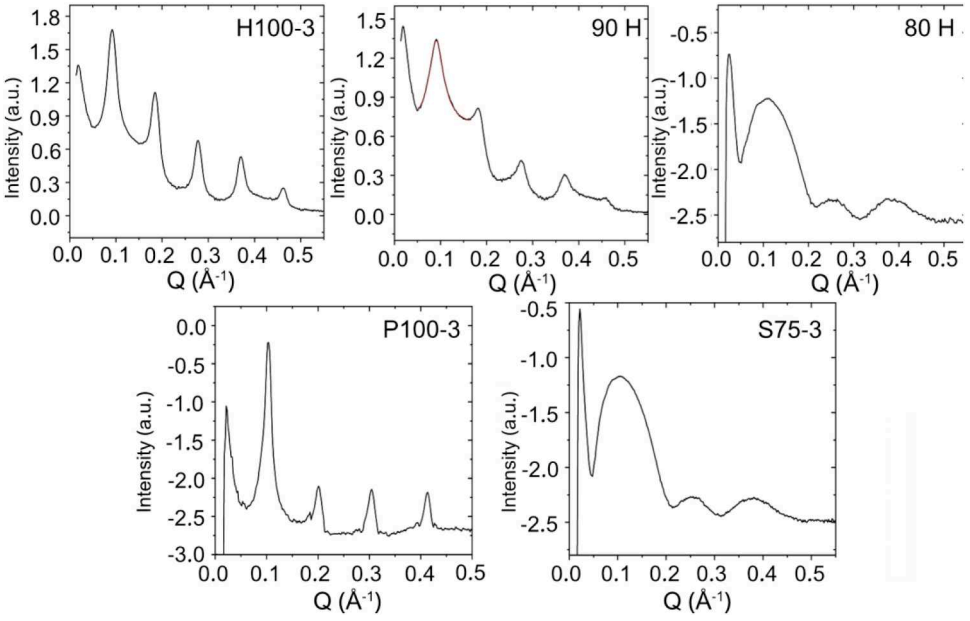

Fig. 6. Small angle X-ray scattering profiles of hydrogenated lecithin mixtures recorded at 20 °C. H100–3, 90 H and P100–3 exhibit a well-defined lamellar phase with at least 4 orders of reflection. 80 H and S75–3 show only wide peaks.

Lu et al., 2016).

Comparable SAXS experiments with non-hydrogenated egg lecithin with 70 % of PCs (E80S) showed a profile formed by a single lamellar phase with d-spacing of 66 Å (Otto et al., 2018).

3.2.2. *Differential scanning calorimetry*

Finally, thermal analysis of the used saturated mixtures was performed using differential scanning calorimetry (DSC). DSC measures differences in heat flow between a sample and a reference, providing information about the thermal behavior, including phase transitions, melting points, and crystallization behavior. The corresponding DSC thermograms are presented in Fig. 7 and the extracted data in Table 5. The pure PCs DPPC and DSPC exhibit two transition peaks in their DSC thermograms. The sharp and high-enthalpy transition is the so-called main-phase transition from the gel state to the liquid-crystalline L_α phase connected with the chain melting process. The temperatures T_m of this transition are at 41.4 °C for DPPC and 54.5 °C for DSPC. The much smaller and broader transition at slightly lower temperatures is the so-called pre-transition from the gel phase $L_{\beta'}$ to the ripple phase $P_{\beta'}$. The main fraction in the studied PCs is composed of a mixture of phospholipids with palmitoyl and stearoyl chains (DPPC, DSPC, PSPC). The sample H100–3 presented a pre-transition at 47.5 °C followed by a sharp

Table 5
The temperatures of the pre- and main-transitions observed in the DSC thermograms of the studied lecithin mixtures (indicated) as well as DPPC and DSPC.

lipid	T_p [°C]	T_m [°C]
H100–3	47.5	52.9
90 H		53.2
80 H		52.6
P100–3	45.3	51.9
S75–3		53.2
DPPC	35.7	41.4
DSPC	51.2	54.5

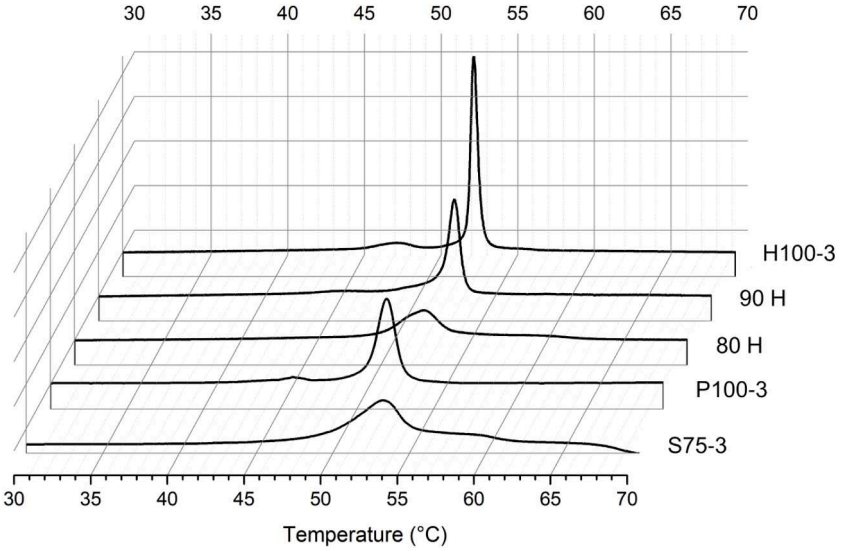

Fig. 7. DSC thermograms of the used lecithin mixtures (indicated).

phase transition from gel to liquid crystalline at 52.9 °C. Although P100–3 in terms of total PC composition is comparable with H100–3, it presents a weaker pre-transition at 45.3 °C and a broader peak at 51.9 °C which may indicate a less homogenous composition in PC chains. As follows, the batch 90 H loses the pre-transition and possessed a wider peak at 53.2 °C, what might be a direct effect of the introduction of new phospholipids into the mixture. Finally, the two batches 80 H and S75–3 show very broad peaks at 52.6 and 53.2 °C, respectively. Moreover, additional heat flux above T_m due to phase separation in the mixture has been detected. The presence of the extra phase transition is in agreement with the SAXS results showing for 80 H and S75–3 the existence of several phases.

3.3. Solubility studies

The measured solubilities reflect the lower limit for complete solubilization (green color code) or the highest dilution without solubilization (red color code) (see Table S2). It has been shown that the hydrogenated PLs studied were highly soluble in the following co-solvents: glycerol, pentylene glycol and transcutol P. These co-solvents are suitable for the incorporation of the studied PLs into relevant dermal formulations. Propylene glycol appears to be of limited relevance. In few cases, very small amounts of insoluble material were found even after excessive dilution. These traces do not dissolve and are, therefore, classified as 'insoluble traces'.

3.4. HLD determination

The calculated CC-values of the natural PLs studied are shown in Table 6. The CC-values of all hydrogenated PLs are higher than 5 showing that these PLs are more lipophilic than Span 20. Therefore, for the incorporation of these PLs into relevant dermal and cosmetic formulation the use of co-solvents is substantial. Furthermore, the results obtained show that the CC-value is a suitable parameter to characterize complex surfactant mixtures such as the plant-based PLs.

Furthermore, it could be shown that the HLB-parameter was not suitable to characterize the studied hydrogenated PLs appropriately, but it still remains the standard for most formulation tasks and is mostly the only value for detergent characteristics in data sheets. CC-values have been collected for a variety of detergents, but unfortunately data sets of both CC-values and HLB-values of one and the same detergent are very limited (see Table 7).

4. Conclusion

Phospholipids are the main component of cell membranes and fundamental components in formulation and development of pharmaceutical and cosmetic products. Important sources of phospholipids are natural products extracted from many sources which can be catalytically converted into hydrogenated lipid compounds. These mixtures are stable at ambient temperature and to light exposure making them ideal products from a stability point of view. Objective of this work was to characterize the physicochemical properties of such lecithins with the analysis of monolayer and bilayer systems. Monolayer studies showed a great resemblance of these mixtures to DSPC, which presents a stiff condensed monolayer with no phase transitions from liquid-expanded to liquid-condensed phases. X-ray scattering analysis revealed that regardless the total content of phosphatidylcholine, all plant-based lecithins presented the same type of structure, a centered rectangular unit cell with NN-tilt. Monolayers of mixtures containing 70 % of phosphatidylcholine were able to attract Ca^{2+} cations showing the presence of a net negative charge in comparison to mixtures with $\geq$ 90 % of phosphatidylcholine which did not attract these cations. Studies on multilayer-systems showed very different behaviour connected to the relative amount of phosphatidylcholine in the plant-based lecithin. H100–3, 90 H and P100–3 formed well-defined lamellar phases with clear phase transitions. Differently, 80 H and S75–3 formed positionally uncorrelated bilayers due to the presence of charged species. In the calorimetric curves broader peaks followed by small extra phase transitions have been observed.

HLD and CPP parameters have been determined as well as the solubility in different co-solvents relevant for the preparation of semisolid and innovative colloidal formulations for dermal and cosmetic applications. It has been shown that the HLD and CPP as macroscopic parameters can be used in order to characterize different natural PLs with varying PC content. Furthermore, it could be demonstrated that the monolayer system at the air/liquid interface is a suitable method to characterize the studied PLs on a supramolecular level.

Table 6
Determined CC values of the natural PLs (EACN and salt scan at 40 °C).

PL	H100–3	P100–3	90 H	80 H	S75–3	DPPC
CC-value	5.0	5.0	5.0	5.6	5.5	4.3

Table 7
Examples for surfactants and their CC/HLB-values.

Substance	CC-value	Source	HLB-value	Source
P100–3	5.0	this work	8.8 – 10.0	(Abbott, 2015/2016)
Tween 80	−3.7	(Otto et al., 2020)	15	DAC/NRF
Span 20	3.5	(Otto et al., 2020)	8.6	DAC/NRF

CRediT authorship contribution statement

Fabio Strati: Writing – original draft, Visualization, Validation, Methodology, Investigation, Formal analysis, Data curation. **Simon Drescher:** Writing – original draft, Data curation. **Chen Shen:** Writing – original draft, Visualization, Validation, Investigation. **Reinhard H.H. Neubert:** Writing – original draft, Funding acquisition, Conceptualization. **Gerald Brezesinski:** Writing – original draft, Supervision, Investigation.

Declaration of competing interest

There are no conflicts of interest to declare.

Acknowledgements

We acknowledge DESY (Hamburg, Germany), a member of the Helmholtz Association HGF, for the provision of experimental facilities. Parts of this research were carried out at PETRA III and we would like to thank Rene Kirchhof and Milena Lippmann for assistance in using P08 and chemistry lab, respectively.

This study was funded by the Phospholipid Research Center Heidelberg. We thank Lipoid GmbH Ludwigshafen for providing the plant-based lecithins. We thank Prof. Thurn-Albrecht and Dr. Petzold from the Physics Department at the Martin Luther University Halle for the access and help with the SAXS experiments. We thank Katrin Herfurt for the assistance with the DSC experiments and Dr. C. Hage for the help with the solubility studies.

Supplementary materials

Supplementary material associated with this article can be found, in the online version, at doi:10.1016/j.ejps.2025.107144.

GIXD contour plots of all used lecithin mixtures recorded at different lateral pressures at 20 °C on 5 mM $CaBr_2$.

Table with all GIXD parameters extracted from the GIXD data.

GIXOS signals of the plant-based PL monolayers at 30 mN/m and the corresponding reconstructed scattering length density profiles SLD(z)

TRXF spectra (fluorescence intensity vs. photon energy) of monolayers of selected plant-based mixtures on subphases containing 5 mM $CaBr_2$.

Solubilities of the studied phospholipids in relevant co-solvents.

Data availability

No data was used for the research described in the article.

References

Abbott, S., 2015/2016. Surfactant science: principles and practice. free eBook 2015, 1–249. S. Abbott, 2021. Practical Surfactants. https://www.stevenabbott.co.uk/practical-surfactants/cc.php.

Acosta, E.J., Yuan, J.S., Bhakta, A.S., 2008. The Characteristic curvature of ionic surfactants. J. Surfactants Deterg. 11, 145–158. https://doi.org/10.1007/s11743-008-1065-7.

Andreeva, T.D., Petrov, J.G., Brezesinski, G., Moehwald, H., 2008. Structure of the Langmuir monolayers with fluorinated ethyl amide and ethyl ester polar heads creating dipole potentials of opposite sign. Langmuir 24, 8001–8007. https://doi.org/10.1021/la8009282.

Brezesinski, G., Kaganer, V.M., Möhwald, H., Howes, P.B., 1998. Structure of octadecanol monolayers: an x-ray diffraction study. J. Chem. Phys. 109, 2006–2010.

Brezesinski, G., Möhwald, H., 2003. Langmuir monolayers to study interactions at model membrane surfaces. Adv. Colloid Interface Sci. 100-102, 563–584.

Brezesinski, G., Müller, H.J., Toca-Herrera, J.L., Krustev, R., 2001. X-ray diffraction and foam film investigations of PC head group interaction in water/ethanol mixtures. Chem. Phys. Lipids 110, 183–194. https://doi.org/10.1016/S0009-3084(01)00135-9.

Brezesinski, G., Schneck, E., 2019. Investigating ions at amphiphilic monolayers with X-ray fluorescence. Langmuir 35, 8531–8542. ttps://doi.org/10.1021/acs.langmuir.9b00191.

Bringezu, F., Dobner, B., Brezesinski, G., 2002. Generic phase behavior of branched-chain phospholipid monolayers. Chem. - Eur. J. 8, 3203–3210. https://doi.org/10.1002/1521-3765(20020715.

Bryant, G., Taylor, M.B., Darwish, T.A., Krause-Heuer, A.M., Kent, B., Garvey, C.J., 2019. Effect of deuteration on the phase behaviour and structure of lamellar phases of phosphatidylcholines – Deuterated lipids as proxies for the physical properties of native bilayers. Colloids Surf. B Biointerfaces 177, 196–203. https://doi.org/10.1016/j.colsurfb.2019.01.040.

Cevc, G., 1993. Phospholipids Handbook. Taylor & Francis, London, UK.

Dahmen-Levison, U., Brezesinski, G., Möhwald, H., Jakob, J., Nuhn, P., 2000. Investigations of lipid - protein interactions on monolayers of chain-substituted phosphatidylcholines. Angew. Chem. - Int. Ed. 39, 2775–2778. https://doi.org/10.1002/1521-3773(20000804.

Dai, Y., Lin, B., M, M., Kim, K., Leahy, B., Shpyrko, O.G., 15 November 2011. A comparative study of Langmuir surfactant films: grazing incidence x-ray off-specular scattering vs. x-ray specular reflectivity. J. Appl. Phys. 110 (10), 102213. https://doi.org/10.1063/1.3661980.

Estrela-Lopis, I., Brezesinski, G., Möhwald, H., 2004. Miscibility of DPPC and DPPA in monolayers at the air/water interface. Chem. Phys. Lipids 131, 71–80. https://doi.org/10.1016/j.chemphyslip.2004.04.005.

G. Fricker, T. Kromp, A. Wendel, A. Blume, J. Zirkel, H. Rebmann, C. Setzer, R. Quinkert, F. Martin, C. Müller-goymann, Phospholipids and lipid-based formulations in oral drug delivery, (2010) 1469–1486. doi:10.1007/s11095-010-0130-x.

M. Fujii, K. Shiozawa, Y. Watanabe, M. Matsumoto, Effect of phosphatidylcholine on skin permeation of indomethacin from gel prepared with liquid paraffin and hydrogenated phospholipid, 222 (2001) 57–64.

Experimental Biology 2017 Meeting Abstracts. FASEB Journal 31, 2017, S1.

Gobley, M., 1850. Recherches Chimiques sur les Oeufs de Carpe. J. Pharm. Chim 17, 401–430.

Hao, C., Liu, Q., Li, Q., Zhang, J., Sun, R., 2016. Thermodynamic and structural studies of DMPC and DSPC with DOTAP mixed monolayers at the air-water interface. Russ. J. Phys. Chem. A 90, 214–219. https://doi.org/10.1134/S0036024415120079.

Israelachvili, J.N., 2015. Intermolecular and Surface Forces. Academic press.

Kaganer, V.M., Brezesinski, G., Möhwald, H., Howes, P.B., Kjaer, K., 1998. Positional order in Langmuir monolayers. Phys. Rev. Lett. 81, 5864–5867.

Kaganer, V.M., Möhwald, H., Dutta, P., 1999. Structure and phase transitions in Langmuir monolayers. Rev. Mod. Phys. 71, 779–819.

Kjaer, K., 1994. Some simple ideas on X-ray reflection and grazing-incidence diffraction from thin surfactant films. Phys. B Phys. Condens. Matter 198, 100–109. https://doi.org/10.1016/0921-4526(94)90137-6.

Kjaer, K., Als-Nielsen, J., Helm, C.A., Laxhuber, L.A., Möhwald, H., 1987. Ordering in lipid monolayers studied by synchrotron x-ray diffraction and fluorescence microscopy. Phys. Rev. Lett. 58, 2224–2227. https://doi.org/10.1103/PhysRevLett.58.2224.

I. Kuzmenko, H. Rapaport, K. Kjaer, J. Als-Nielsen, I. Weissbuch, M. Lahav, L. Leiserowitz, Design and characterization of crystalline thin film architectures at the air − liquid interface : simplicity to complexity, (2001). doi:10.1021/cr990038y.

Lantz, R.A., 1989. Industrial methods of analysis. Lecithins Sources, Manuf. Uses. B. F., pp. 162–173

Lu, B.-S., Gupta, S.P., Belicka, M., Podgornik, R., Pabst, G., 2016. Modulation of elasticity and interactions in charged lipid multibilayers: monovalent salt solutions. Langmuir 32, 13546–13555.

Lúcio, M., Bringezu, F., Reis, S., Lima, J.L.F.C., Brezesinski, G., 2008. Binding of nonsteroidal anti-inflammatory drugs to DPPC: structure and thermodynamic aspects. Langmuir 24, 4132–4139. https://doi.org/10.1021/la703584s.

A.R. Machado, L.M. De Assis, M. Inês, R. Machado, Importance of lecithin for encapsulation processes, 8 (2014) 176–183. doi:10.5897/AJFS2013.1092.

Möhwald, H., Brezesinski, G., 2016. From langmuir monolayers to multilayer films. Langmuir 32, 10445–10458. https://doi.org/10.1021/acs.langmuir.6b02518.

Mukhina, T., Pabst, G., Ruysschaert, J.-M., Brezesinski, G., Schneck, E., 2022. pH-dependent physicochemical properties of ornithine lipid in mono- and bilayers. Phys. Chem. Chem. Phys. 24, 22778–22791.

Nastruzzi, C., Esposito, E., Menegatti, E., Walde, P., 1993. Use and stability of liposomes in dermatological preparations. J. Appl. Cosmetol. 11, 77–91.

Nguyen, T.T.L., Edelen, A., Neighbors, B., Sabatini, D.A., 2010. Biocompatible lecithin-based microemulsions with rhamnolipid and sophorolipid biosurfactants: formulation and potential applications. J. Colloid Interface Sci. 348, 498–504. https://doi.org/10.1016/j.jcis.2010.04.053.

Otto, F., van Hoogevest, P., Syrowatka, F., Heinl, V., Neubert, R.H.H., 2020. Assessment of the applicability of HLB values for natural phospholipid emulsifiers for preparation of stable emulsions. Pharmazie 75, 365–370.

Otto, F., Brezesinski, G., van Hoogevest, P., Neubert, R.H.H., 2018. Physicochemical characterization of natural phospholipid excipients with varying PC content. Colloids Surf. A 291–296.

Pepeu, G., Vannucchi, M.G., Di Patre, P.L., 1990. Pharmacological actions of phospholipids. In: Hanin, I., Pepeu, G. (Eds.), Phospholipids Biochem. Pharm. Anal. Considerations. Springer US, Boston, MA, pp. 43–50. https://doi.org/10.1007/978-1-4757-1364-0_3.

Perkins, E.G., 1995. Chapter 2 - composition of soybeans and soybean products. In: Erickson, D.R. (Ed.), Pract. Handb. Soybean Process. Util. AOCS Press, pp. 9–28. https://doi.org/10.1016/B978-0-935315-63-9.50006-1.

Pozo-Navas, B., Raghunathan, V., Katsaras, J., Rappolt, M., Lohner, K., Pabst, G., 2003. Discontinuous unbinding of lipid multibilayers. Phys. Rev. Lett. 91, 028101.

Pryde, E.H., American Oil Chemists' Society, 1985. Chemical reactions of phosphatides. No title. In: Lecithins, 1. Szuha, B.F, Champaign, IL, USA, pp. 213–246.

Pusterla, J., Scoppola, E.A.C., Mukhina, T., Shen, C., Brezesinski, G., Schneck, E., 2022. Characterization of lipid bilayers adsorbed to functionalized air/water interfaces. Nanoscale 14, 15048–15059. https://doi.org/10.1039/D2NR03334H.

Seeck, O.H., Deiter, C., Pflaum, K., Bertam, F., Beerlink, A., Franz, H., Horbach, J., Schulte-Schrepping, H., Murphy, B.M., Greve, M., Magnussen, O., 2012. The high-resolution diffraction beamline P08 at PETRA III. J. Synchrotron Rad. 19, 30–38. https://doi.org/10.1107/S0909049511047236.

Senior, G., Gregoriadis, J., 1982. Printed in the U.S.A. Pergamon Press stability of small unilamellar liposomes in serum and clearance from the circulation : the effect of the phospholipid and cholesterol components. Judith Sr. Greg. Gregor. Div. Clin. Sci. 30, 2123–2136.

V.L. Shapovalov, M.E. Ryskin, O.V. Konovalov, A. Hermelink, G. Brezesinski, Elemental analysis within the electrical double layer using total reflection X-ray fluorescence technique, (2007) 3927–3934. doi:10.1021/jp066894c.

Shen, C., Zhang, H., Ocko, B.M., 2024. Reconstructing the reflectivity of liquid surfaces from grazing incidence X-ray off-specular scattering data. J. Appl. Cryst. 57, 714–727. https://doi.org/10.1107/S1600576724002887.

Shinoda, T., Kaneko, K., 1988. Characteristic properties of Lecithin AS a surfactant. J. Dispers. Sci. Technol. 9, 555–559.

Stefaniu, C., Brezesinski, G., 2014. X-ray investigation of monolayers formed at the soft air/water interface. Curr. Opin. Colloid. Interface Sci. 19, 216–227. https://doi.org/10.1016/j.cocis.2014.01.004.

Stefaniu, C., Brezesinski, G., Möhwald, H., 2014. Langmuir monolayers as models to study processes at membrane surfaces. Adv. Colloid Interface Sci. 208, 197–213. https://doi.org/10.1016/j.cis.2014.02.013.

Sturm, M., Gutowski, O., Brezesinski, G., 2019. The influence of calcium traces in ultrapure water on the lateral organization in tetramyristoyl cardiolipin monolayers. Chemphyschem. 20, 1521. https://doi.org/10.1002/cphc.201900126[36.

T.F. Tadros, 2016, Emulsions: formation, stability, industrial applications. 1st ed., De Gruyter, Berlin; Abbott, S., 2015/2016. Surfactant Science: Principles and Practice. free eBook 2015:1-249.

Van Hoogevest, P., Liu, X., Fahr, A., Leigh, M.L.S., 2011. Role of phospholipids in the oral and parenteral delivery of poorly water soluble drugs. J. Drug Deliv. Sci. Technol. 21, 5–16. https://doi.org/10.1016/S1773-2247(11)50001-2.

Van Hoogevest, P., Wendel, A., 2014. The use of natural and synthetic phospholipids as pharmaceutical excipients. Eur. J. Lipid Sci. Technol. 116, 1088–1107. https://doi.org/10.1002/ejlt.201400219.

Wendel, A., 2014. Lecithin. Kirk-Othmer Encycl. Chem. Technol. American Cancer Society, pp. 1–19. https://doi.org/10.1002/0471238961.1205030923051404.a01.pub2.

Wiegart, L., Struth, B., Tolan, M., Terech, P., 2005. Thermodynamic and structural properties of phospholipid langmuir monolayers on hydrosol surfaces. Langmuir 21 (16), 7349–7357. https://doi.org/10.1021/la050478m.